

Protracted Kondo screening and kagome bands in heavy-fermion metal Ce_3Al

Li Huang^{1,*} and Haiyan Lu¹

¹*Science and Technology on Surface Physics and Chemistry Laboratory, P.O. Box 9-35, Jiangyou 621908, China*
(Dated: February 6, 2022)

Ce_3Al is an archetypal heavy-fermion compound with multiple crystalline phases. Here, we try to investigate its electronic structures in the hexagonal phase ($\alpha\text{-Ce}_3\text{Al}$) and cubic phase ($\beta\text{-Ce}_3\text{Al}$) by means of a combination of density functional theory and single-site dynamical mean-field theory. We confirm that the $4f$ valence electrons in both phases are itinerant, accompanied with strong valence state fluctuations. Their $4f$ band structures are heavily renormalized by electronic correlations, resulting in large effective electron masses. The Kondo screening in Ce_3Al would be protracted over a wide range of temperature since the single-impurity Kondo temperature T_K is much higher than the coherent Kondo temperature T_K^* . Especially, the crystal structure of $\alpha\text{-Ce}_3\text{Al}$ forms a layered kagome lattice. We observe conspicuous kagome-derived flat bands and Dirac cones (or gaps) in its quasiparticle band structure. Therefore, it is concluded that the hexagonal phase of Ce_3Al will be a promising candidate of heavy-fermion kagome metal.

I. INTRODUCTION

The discovery of fully gapped d -wave superconductivity in CeCu_2Si_2 has triggered a great deal of interests in heavy-fermion materials¹⁻⁵. These materials are typically intermetallic compounds containing rare earths (Ce, Sm, and Yb) or actinides (U, Np, and Pu). They exhibit a barrage of unusual properties that we still don't fully understand. For example, in comparison to normal metals, they have enormous values of effective electron masses m^* , linear specific heat coefficients γ , and low-temperature magnetic susceptibilities χ ⁶. Even more fascinating, the heavy-fermion materials host a plethora of atypical phenomena and exotic quantum states, including quantum criticality, unconventional superconductivity, non-Fermi-liquid state, topological Kondo insulator and topological Kondo semimetal⁷⁻¹², just to name a few. Due to these tantalizing properties, the search for and characterization of heavy-fermion materials have become a rapid growing field in the condensed matter physics.

It is worth noting that quite a large portion of heavy-fermion materials are cerium-based intermetallic compounds¹³. They have attracted more attentions than the other uranium-based and ytterbium-based heavy-fermion compounds⁶. For example, CeCu_2Si_2 is the first known heavy-fermion superconductor¹, as mentioned before. However, after 40 years, the exact symmetry of its superconducting gap has not been settled yet¹⁴⁻¹⁶. CeCoIn_5 is another heavy-fermion superconductor with a relatively high T_c ($T_c > 2.3$ K). Besides unconventional superconductivity, it also exhibits spin-density-wave magnetic ordering¹⁷, Fulde-Ferrell-Larkin-Ovchinnikov state¹⁸, and antiferromagnetic quantum critical point¹⁹⁻²¹, which can be easily modulated by external conditions, such as temperature, pressure, magnetic field, and chemical doping. Recently, it is used as a testbed to unveil the quasiparticle dynamics (collective hybridization between localized $4f$ moments and conduction electrons) at $T > T^*$, where T^* marks the heavy-fermion coherence temperature²². The third example concerns the cerium-based heavy-fermion topological semimetals, which provide a promising setting to study topological semimetals²³ driven by electronic correlations. For instance, $\text{Ce}_3\text{Bi}_4\text{Pd}_3$, a heavy-fermion system without centrosymmetry and magnetic

order, is newly found to be a realization of the so-called Weyl-Kondo semimetal^{7,24,25}, which features strongly renormalized Weyl nodes in the bulk and hosts Fermi arcs on the surface.

Now let us turn to the cerium-aluminium heavy-fermion system Ce_xAl_y . It contains at least four stable intermetallic compounds, specifically, CeAl_y ($y = 1, 2, 3$) and Ce_3Al . The ground states of CeAl and CeAl_2 are antiferromagnetic, which are quite complicated. Below 3.5 K, CeAl_2 enters an antiferromagnetic phase, in which the magnitudes and directions of the magnetic moments exhibit spatial periodicity. It is generally believed that this spin-density-wave-like antiferromagnetic ordering develops out of hybridization between localized $4f$ spins and conduction electrons (Kondo effect)²⁶. CeAl_3 is known to be the first discovered heavy-fermion metal with tremendous magnitude of the linear specific heat term [$\gamma = 1620 \text{ mJ} / (\text{mole} \cdot \text{K}^2)$]²⁷. Its ground state is also antiferromagnetic with $T_N = 1.2 \text{ K}$ ²⁸. As for Ce_3Al , at room temperature it crystallizes into a hexagonal Ni_3Sn -type structure [i.e. $\alpha\text{-Ce}_3\text{Al}$, see Fig. 1(a)]. Above 500 K, it transforms into a cubic Cu_3Au -type structure [i.e. $\beta\text{-Ce}_3\text{Al}$, see Fig. 1(c)]. Below 115 K, another structural phase transition occurs and the monoclinic γ phase appears. The antiferromagnetic ordering develops below 2.5 K ²⁹. Previous studies have revealed fingerprints of heavy fermions in the thermodynamic, magnetic, and transport properties in Ce_3Al ³⁰⁻³². Strictly, Ce_3Al is classified as a heavy-fermion system because of the large linear specific heat coefficient [$\gamma = 85 \sim 114 \text{ mJ} / (\text{mole Ce} \cdot \text{K}^2)$]³³, but its $4f$ electrons are not as heavy as those in CeAl_y ^{30,31}.

Among the intermetallic compounds made by Ce and Al, CeAl_2 and CeAl_3 have been most extensively studied in relation to their magnetic and heavy-fermion properties²⁶⁻²⁸. On the other hand, only a few works have been reported for Ce_3Al ²⁹⁻³². Consequently, we know a little about the detailed electronic structures of Ce_3Al . The variation of the $4f$ electronic states across the three phases remains unknown so far. Therefore, in the present work, we make a systematic study about the electronic structures of the high-symmetry phases of Ce_3Al ($\alpha\text{-Ce}_3\text{Al}$ and $\beta\text{-Ce}_3\text{Al}$) by means of a state-of-the-art first-principles many-body approach. We try to calculate the quasiparticle band structures, density of states, self-energy functions, and valence state histograms of both phases. The Kondo temperatures and effective electron masses are also

measured. Our results discover that the $4f$ electrons in both phases are itinerant and fluctuating heavily among various electronic configurations, but they are not coherently screened by conduction electrons to form a Fermi-liquid state³⁴ in the temperatures that we are interested in. In addition, it is suggested that α - Ce_3Al is a prototype of kagome metal, which is characterized by the coexistence of dispersionless and linearly dispersive energy bands³⁵.

The rest of this paper is organized as follows. Firstly, the computational details are introduced in section II. Then in section III, the major results, including the momentum-resolved spectral functions, density of states, Kondo temperatures, self-energy functions, and valence state histograms of the two phases are presented and analyzed. Section IV is devoted to discuss the kagome-derived flat bands and Dirac cones (or gaps) in the quasiparticle band structure of α - Ce_3Al . Finally, section V serves as a short summary.

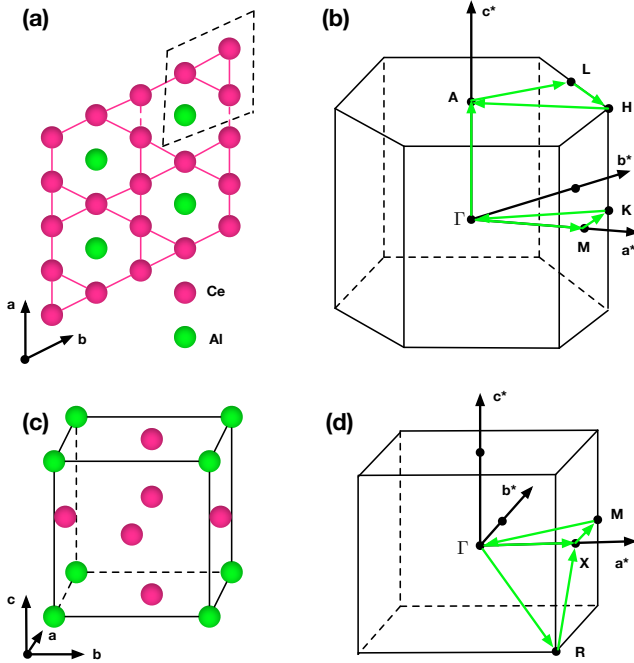


FIG. 1. (Color online). (a) and (c) Crystal structures of α - and β - Ce_3Al . Here, Ce and Al atoms are represented by red and green balls, respectively. In panel (a), only the kagome layer is illustrated, and the dashed rhomboid means the unit cell. (b) and (d) Schematic pictures for Brillouin zones of α - and β - Ce_3Al . Some selected high-symmetry directions are labelled.

II. METHOD

In the present work, we employed the single-site dynamical mean-field theory in combination with the density functional theory (dubbed DFT + DMFT)^{36,37} to study the electronic structures of α - and β - Ce_3Al . Notice that this method has been successfully applied to explore the physical properties of many cerium-based heavy-fermion materials^{38–43}.

The DFT calculations were done by using the WIEN2K code, which implements a full-potential linearized augmented plane-wave formalism⁴⁴. We adopted the experimental crystal structures^{30,32}. The muffin-tin radii for Ce and Al atoms were 2.5 and 2.4 a.u., respectively. $R_{\text{MT}} \times K_{\text{MAX}} = 7.0$. The Perdew-Burke-Ernzerhof functional⁴⁵, i.e. the generalized gradient approximation was adopted to express the exchange-correlation potential. The k -meshes for Brillouin zone integrations for the α - and β - Ce_3Al phases were $15 \times 15 \times 16$ and $15 \times 15 \times 15$, respectively. The spin-orbit coupling was considered in all calculations explicitly.

Since the electronic correlations among Ce's $4f$ valence electrons are crucial, we have to taken them into accounts. We utilized the DMFT method to treat the correlated nature of $4f$ electrons. Here, we used the eDMFT code developed by K. Haule⁴². The system temperatures for α - and β - Ce_3Al were set to be $T \approx 230$ K ($\beta = 50.0$) and $T \approx 580$ K ($\beta = 20.0$), respectively. A large energy window (from -10 eV to +10 eV with respect to the Fermi level) was used to construct the DMFT projectors and local orbitals. The Coulomb repulsion interaction parameter U and Hund's exchange interaction parameter J_H for Ce's $4f$ electrons were 6.0 eV and 0.7 eV, respectively^{39–43}. The double counting term for the self-energy functions was subtracted via the exact scheme⁴⁶. In order to solve the auxiliary quantum impurity problems for $4f$ electrons, a hybridization expansion continuous-time quantum Monte Carlo impurity solver (dubbed CT-HYB)^{47–49} was used. For each quantum impurity solver run, the number of Monte Carlo steps was up to 200 million per CPU process. We performed charge fully self-consistent DFT + DMFT calculations. In order to obtain good convergence, the maximum number of DFT + DMFT iterations was set to 100.

III. RESULTS

Quasiparticle band structures. The momentum-resolved spectral functions (or equivalently quasiparticle band structures) $A(\mathbf{k}, \omega)$ along some selected high-symmetry directions for the α and β phases of Ce_3Al are visualized in Fig. 2(a) and (d), respectively. The spectra of the two phases share some common characteristics. At first, the spectra below the Fermi level look quite coherent and have large dispersions, which are attributed to the contributions of conduction electrons. Secondly, the incoherent $4f$ bands dominate above the Fermi level, resulting in blur and diffused spectra. Thirdly, we observe remarkable stripe-like features near the Fermi level. One stripe pins exactly at the Fermi level, while the other is a few hundred meV above the Fermi level. These stripes are related with the spin-orbit splitting $4f_{5/2}$ and $4f_{7/2}$ bands, which have been seen in Ce metal⁴⁰ and some other cerium-based heavy-fermion compounds, such as CeTiIn_5 ^{39,42}, CeIn_3 ⁴³, CeB_6 ⁵⁰, and CeM_2Si_2 ⁴¹. The low-lying $4f_{5/2}$ bands are extremely flat and intense, leading to sharp peaks at the Fermi level in the density of states. They signal the itinerant behaviors of $4f$ electrons in α - and β - Ce_3Al .

Fig. 2(b) and (e) depict the total density of states $A(\omega)$ and $4f$ partial density of states $A_{4f}(\omega)$. $A_{4f}(\omega)$ shows promi-

TABLE I. Important model parameters for the electronic structures of α -Ce₃Al and β -Ce₃Al. They include the width of conduction band below the Fermi level (W), the averaged $4f$ electron level (ϵ_f), the imaginary part of hybridization function at the Fermi level [$\text{Im}\Delta(E_F)$], the density of states of conduction electrons at the Fermi level [$\rho_c(E_F)$], the Kondo temperature (T_K), the coherent Kondo temperature (T_K^*), the quasiparticle weights ($Z_{5/2}$ and $Z_{7/2}$), the effective electron masses ($m_{5/2}^*$ and $m_{7/2}^*$), and probabilities of $4f^0$, $4f^1$, and $4f^2$ configurations (p_0 , p_1 , and p_2). See main texts for more details.

cases	W	ϵ_f^a	$\text{Im}\Delta(E_F)^b$	$\rho_c(E_F)$	T_K	T_K^*	$Z_{5/2}$	$Z_{7/2}$	$m_{5/2}^*$	$m_{7/2}^*$	p_0	p_1	p_2
α -Ce ₃ Al	7.05 eV	-1.60 eV	-0.147 eV	8.37 eV ⁻¹	684 K	56 K	0.17	0.41	5.88 m_e	2.45 m_e	8.56%	85.36%	6.01%
β -Ce ₃ Al	6.60 eV	-1.46 eV	-0.149 eV	4.23 eV ⁻¹	885 K	47 K	0.13	0.27	7.75 m_e	2.56 m_e	7.21%	87.78%	4.96%

^a $\epsilon_f = [\epsilon_f(j = 5/2) + \epsilon_f(j = 7/2)]/2$.

^b Only for the $4f_{5/2}$ states.

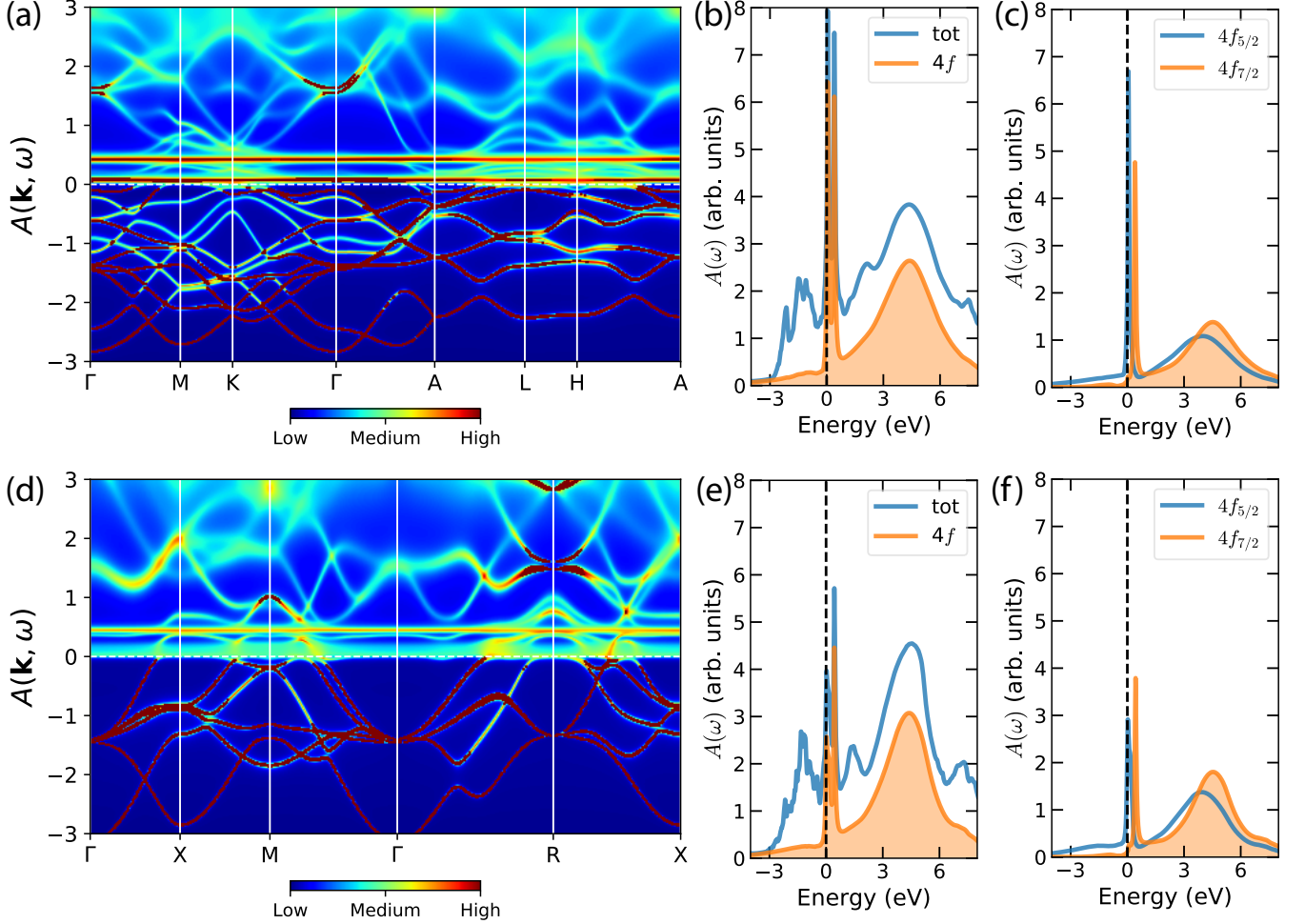


FIG. 2. (Color online). Quasiparticle band structures of Ce₃Al obtained via DFT + DMFT calculations. The results for the α and β phases of Ce₃Al are plotted in the upper and lower panels, respectively. (a) and (d) Momentum-resolved spectral functions $A(\mathbf{k}, \omega)$. (b) and (e) Total and $4f$ partial density of states [i.e. $A(\omega)$ and $A_{4f}(\omega)$]. (c) and (f) j -resolved $4f$ partial density of states [i.e. $A_{4f_{5/2}}(\omega)$ and $A_{4f_{7/2}}(\omega)$]. Here, the horizontal or vertical dashed lines denote the Fermi level. The data of $A(\omega)$, $A_{4f}(\omega)$, $A_{4f_{5/2}}(\omega)$, and $A_{4f_{7/2}}(\omega)$ are rescaled for a better view.

nent three-peaks structure, which is typical in strongly correlated metals³⁷. The Absiksov-Suhl-like quasiparticle peak (or Kondo resonance peak) is well developed at the Fermi level. Due to the spin-orbit coupling effect, it is split into two sub-peaks, which are counterparts of the stripe-like structures as seen in $A(\mathbf{k}, \omega)$. In addition, there is a broad and

smooth “hump” at $2 \text{ eV} < \omega < 8 \text{ eV}$. It is mainly assigned to the upper Hubbard bands of cerium’s $4f$ orbitals. On the other hand, the lower Hubbard bands (residing from -3 eV to -0.5 eV) exhibit small spectral weights, which is consistent with the fact that most of cerium’s $4f$ orbitals are unoccupied. In Fig. 2(c) and (f), we further show the j -resolved

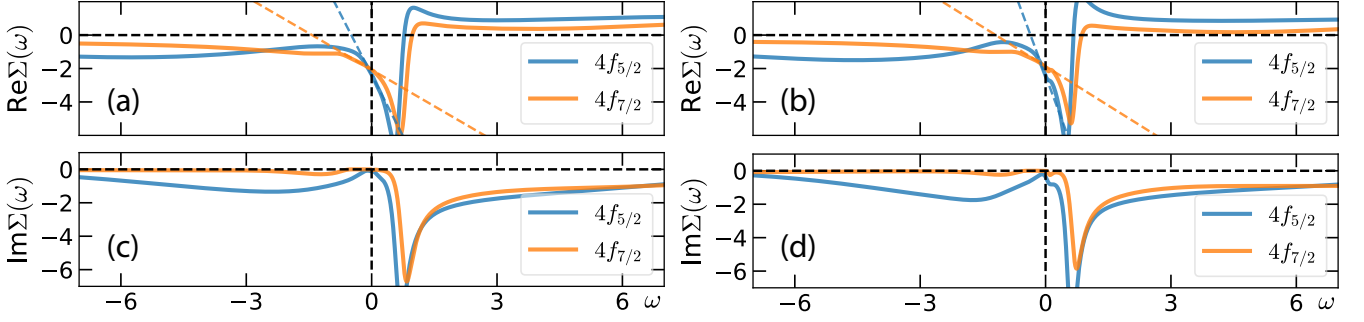


FIG. 3. (Color online). Real and imaginary parts of self-energy functions of Ce-4f electrons at real axis. (a) and (c) α -Ce₃Al. (b) and (d) β -Ce₃Al. In panels (a) and (b), the blue and yellow dashed lines are linear fitting for the low-frequency quasi-linear regimes of the self-energy functions. See main text for more explanations.

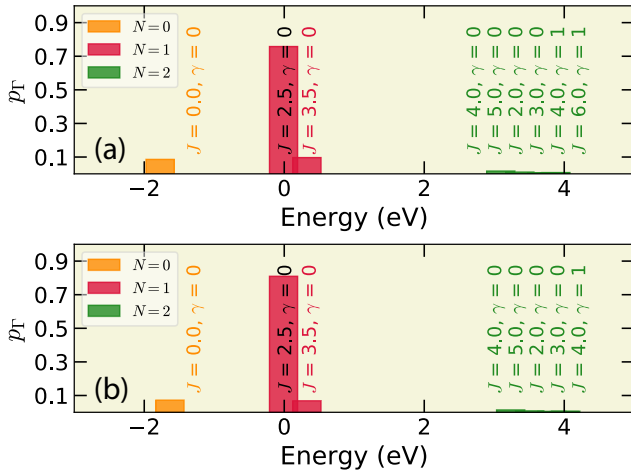


FIG. 4. (Color online). Valence state histograms of Ce's 4f electrons. The data for $4f^3$ ($N = 3$) configurations are too trivial to be seen in this figure. (a) α -Ce₃Al. (b) β -Ce₃Al.

$4f$ partial density of states. We find that the energy separation between the $4f_{5/2}$ and $4f_{7/2}$ peaks is about 350 meV, which is somewhat larger than those in the other cerium-based heavy-fermion compounds^{41–43}. Here we are going to introduce a new variable R . It is the ratio of heights of the two spin-orbit splitting peaks, i.e. $R \equiv h(4f_{5/2})/h(4f_{7/2})$. We find that $R > 1.0$ for α -Ce₃Al, while $R < 1.0$ for β -Ce₃Al. This difference can be easily explained by the temperature effect. When the temperature is increased, the $4f$ electrons should become more and more incoherent^{38,39}. Thus, the low-lying $4f_{5/2}$ bands are suppressed, so does R .

Kondo screening. The physical properties of heavy-fermion materials are controlled by two essential factors⁶. One is the electronic correlations among the localized f electrons, another one is the hybridization (coupling) between localized f electrons (localized f moments) and conduction electrons. In the weak hybridization limit, the Ruderman-Kittel-Kasuya-Yosida (RKKY) interaction dominates, which drives the localized f electrons to yield magnetic ordering states. On the other hand, when the hybridization is strong, the Kondo

mechanism begins to work. The localized moments of f electrons are screened by conduction electrons, and a heavy Fermi-liquid state appears at low temperature. Traditionally, the Kondo temperature is defined to mark the energy scale of screening of a localized f electron. We can use the following equation to make a rough estimation about the single-impurity Kondo temperature T_K ⁵¹:

$$T_K = \sqrt{W|\text{Im}\Delta(E_F)|} \exp\left(-\frac{\pi|\epsilon_f|}{2N_f|\text{Im}\Delta(E_F)|}\right). \quad (1)$$

Here W means that width of occupied conduction bands, $\text{Im}\Delta(E_F)$ means the imaginary part of hybridization function at the Fermi level, ϵ_f is the averaged impurity level for $4f_{5/2}$ and $4f_{7/2}$ states, N_f is the band degeneracy of f electrons. Since the Kondo resonance peak in the Fermi level is mainly associated with the six-fold $4f_{5/2}$ states, $N_f = 6$ in Eq. (1). We can further evaluate the coherent Kondo temperature (or protracted Kondo screening temperature) T_K^* , which indicates the temperature that all localized f electrons are screened by conduction electrons. Note that T_K^* is related to T_K via the following formula^{34,52}:

$$T_K^* = \frac{\rho_c(E_F)}{N_f} T_K^2, \quad (2)$$

where $\rho_c(E_F)$ denotes the density of states of conduction electrons at the Fermi level. We tried to calculate T_K and T_K^* for α - and β -Ce₃Al with Eq. (1) and (2). The calculated results, together with the necessary parameters, are summarized in Table I. Nozières' exhaustion theory³⁴ argues that only those conduction electrons within the Kondo energy scale around the Fermi level E_F can contribute to the screening. As a consequence, the coherent Kondo temperature T_K^* could be much lower than the single-impurity Kondo temperature T_K in heavy-fermion materials with low carrier density⁵³. Our results clearly reveal that $T_K \gg T_K^*$, which suggests that both phases are in the protracted Kondo screening states ($T_K > T > T_K^*$)⁵². The low-temperature resistivity of α -Ce₃Al exhibits two characteristic maximums around 100 K and 3 K, and a minimum around 20 K. The high-temperature anomaly may be due to the $\alpha - \gamma$ phase transition, and the low-temperature

anomaly may originate from the occurrence of antiferromagnetic order. As for the resistance minimum, previous studies suggested that it marks the onset of the Kondo screening (Kondo minimum)^{29,30,33}. Instead, we believe that it denotes a phase transition from the protracted Kondo screening state to the coherent Kondo screening state.

Self-energy functions. Next, let us examine the heavy-fermion states in Ce₃Al. At first, we have to perform analytical continuation for the self-energy functions at Matsubara axis $\Sigma(i\omega_n)$ via the maximum entropy method⁵⁴. The obtained self-energy functions at real axis $\Sigma(\omega)$ are shown in Fig. 3. We find that the orbital differentiation in the self-energy functions is considerable. For the imaginary parts of self-energy functions $\text{Im}\Sigma(\omega)$, sizable gaps occur at $\omega = 0$ for the $4f_{7/2}$ states, indicating their insulating-like nature. However, $|\text{Im}\Sigma(\omega)|$ for the $4f_{5/2}$ states is finite. It means the existence of low-energy electron scattering. For the real parts of self-energy functions $\text{Re}\Sigma(\omega)$, we observe quasi-linear behaviors in the vicinity of the Fermi level. Therefore, we can utilize the following equation to evaluate the quasiparticle weights Z and effective electron masses m^* ³⁷:

$$Z^{-1} = \frac{m^*}{m_e} = 1 - \left. \frac{\partial \text{Re}\Sigma(\omega)}{\partial \omega} \right|_{\omega=0}. \quad (3)$$

The calculated results are tabulated in Table I. Just as expected, the $4f$ electron correlation is orbital-dependent. The low-lying $4f_{5/2}$ states are more correlated than the high-lying $4f_{7/2}$ states ($Z_{5/2} < Z_{7/2}$), so the $4f$ electrons in the $j = 5/2$ states suffer more renormalization and become heavier. It is not surprised that the $4f$ electrons in Ce₃Al are much lighter than those in the other Ce-Al intermetallic heavy-fermion compounds. After all $\gamma_{\text{Ce}_3\text{Al}}/\gamma_{\text{CeAl}_3} \approx 0.2$ ^{27,33}.

Valence state histograms. Valence fluctuation and mixed-valence behavior are general features in correlated f -electron systems^{40,42}. Especially, when the f electrons reside in the itinerant side (strong hybridization limit), these effects will become more prominent⁴⁰. In this work, we tried to calculate the valence state histograms (i.e. atomic eigenstates probabilities) of Ce₃Al to quantify its valence fluctuation⁴⁷. See Fig. 4 for the histograms. Here, we use three good quantum numbers to label these atomic eigenstates, i.e., total occupancy N , total angular momentum J , and γ which stands for the rest of the atomic quantum numbers, such as J_z . We have the following findings. At first glance, the distributions of valence state histograms of α - and β -Ce₃Al are quite similar. They are diverse. Accordingly, the valence state fluctuations in both phases are intense. Second, the probability of $4f^1$ configuration is undoubtedly overwhelming. But the contributions from the other configurations, such as $4f^0$ and $4f^2$, are also crucial (see Table I). The contributions from $4f^3$ and those with more $4f$ occupancies are trivial. With these information, we can easily calculate the expected $4f$ occupancy $\langle N \rangle$ and expected total angular momentum $\langle J \rangle$. For α -Ce₃Al, $\langle N \rangle \approx 0.976$ and $\langle J \rangle \approx 2.47$. While for β -Ce₃Al, $\langle N \rangle \approx 0.978$ and $\langle J \rangle \approx 2.46$. These data are quite close. Third, the ground states of both phases are $|N = 1, J = 2.5, \gamma = 0\rangle$, which is the same with Ce and most of the cerium-based heavy-fermion systems^{41,43,50}. It accounts for 75.7% for α -Ce₃Al and 80.9% for β -Ce₃Al.

Finally, note that the data presented here are quite analogous to those of α -Ce ($\langle N \rangle \approx 0.98$, $\langle J \rangle \approx 2.45$, and the probability of $|N = 1, J = 2.5, \gamma = 0\rangle$ is approximately 68.31%)^{40,47}, in which the $4f$ electrons are known to be itinerant and strongly hybridize with conduction electrons. So, to some extent, the $4f$ electronic structures of Ce₃Al and α -Ce are similar.

IV. DISCUSSION

Very recently, the concept of kagome lattice and kagome metals have attracted quite a lot of attentions³⁵. The kagome lattice or kagome pattern is a two-dimensional network of trihexagonal tiling. If conductive materials are made to resemble some kind of kagome lattice at the atomic scale, they are the so-called kagome metals. From the viewpoint of band topology, the signature of kagome metals is the coexistence of kagome-derived dispersionless flat bands and band crossings between two linearly dispersive bands (i.e. Dirac cones)^{55–57}. When the spin-orbit coupling is nontrivial, Dirac gaps are opened and massive Dirac fermions emerge⁵⁸. Thus, the kagome metals provide ideal platforms to study the interplay between topology and electronic correlation. Up to now, most of the available kagome metals are correlated d -electron systems, containing Fe, Co, and Mn transition metal elements^{55–68}. To our knowledge, the f -electron kagome metals are still absent. It would be interesting to search kagome metals in rare earth and actinide compounds, especially in cerium-based heavy-fermion materials.

Notice that the crystal structure of α -Ce₃Al can be viewed as a sequence stacking of a kagome layer along the c axis [see Fig. 1(a)]. Its kagome layer consists of Ce atoms and the centers of the hexagons are populated by Al atoms. As compared to the other kagome metals^{56,58,67,69}, there is no spacing layer in α -Ce₃Al. Nevertheless, a question is naturally raised. Is α -Ce₃Al a candidate of the heavy-fermion kagome metal? In other words, can we observe kagome-derived flat bands and Dirac cones simultaneously in the electronic structure of α -Ce₃Al? In order to answer this question, we made a further analysis about the DFT + SOC and DFT + DMFT band structures of α -Ce₃Al.

In order to exclude the effect of electronic correlation, we at first carried out DFT and DFT + SOC calculations for α -Ce₃Al. Fig. 5 shows the calculated band structure. We see that, the extremely flat bands, which are largely attributed to the $4f$ orbitals of Ce atoms, spread over the whole Brillouin zone. At the high-symmetry K and H points, there are some crossing points made by linearly dispersive bands. In Fig. 5(a), some representative flat bands and Dirac cones (or Dirac gaps) near the Fermi level are annotated by arrows. Enlarged views for these subtle band structures are illustrated in Fig. 5(b) and (c), and Fig. 6(a) and (b). The Dirac cones at K point have a $4f$ character. They are opened by the spin-orbit coupling to yield two Dirac gaps Δ_1 and Δ_2 . Interestingly, the spin-orbit coupling leads to a converse consequence at the H point. It closes a Dirac gap and recovers a Dirac cone [labelled by DC in Fig. 6(b)]. Anyway, all these characteristics suggest that α -Ce₃Al is a candidate of the kagome metal with heavy

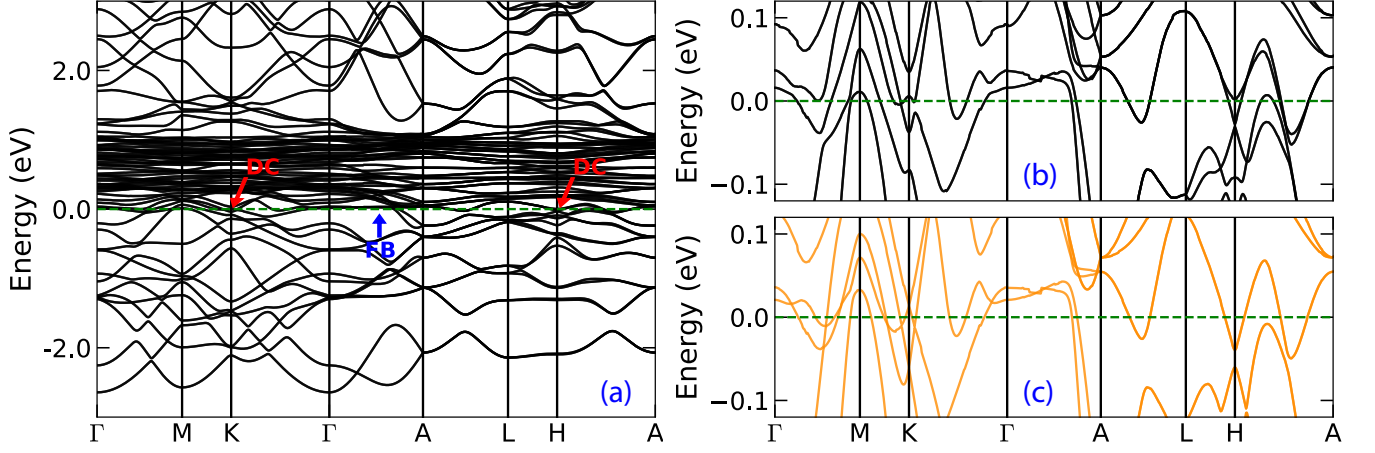


FIG. 5. (Color online). (a) and (b) Electronic band structures of α -Ce₃Al obtained via DFT + SOC calculations. (c) Electronic band structure of α -Ce₃Al obtained via DFT calculations. Here DC means Dirac cone and FB is an abbreviation of flat band. The horizontal dashed line denotes the Fermi level. Note that the Dirac cones or gaps at K and H points should be tuned by spin-orbit coupling.

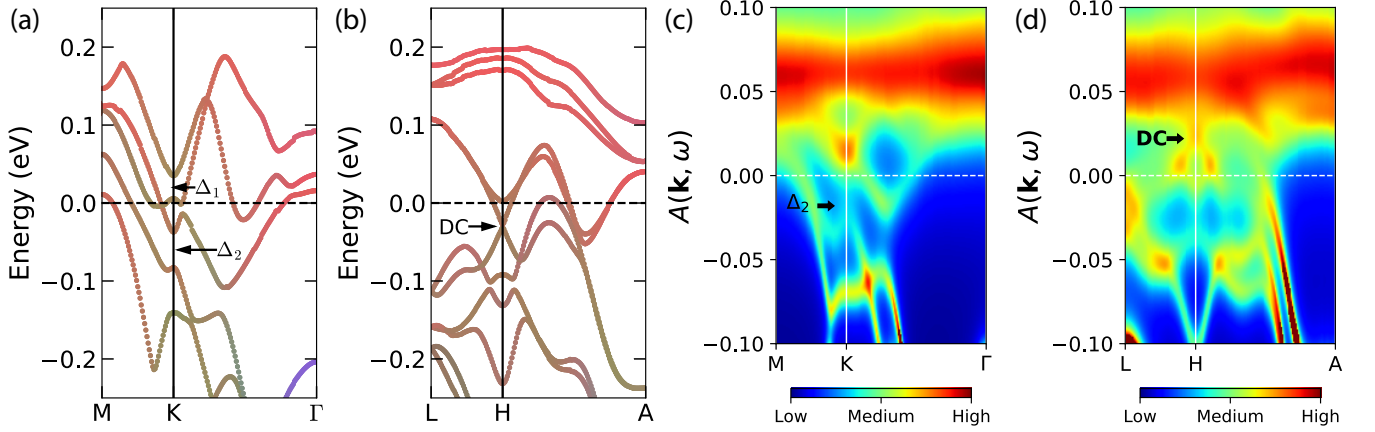


FIG. 6. (Color online). (a) and (b) DFT + SOC band structures for α -Ce₃Al in some selected high-symmetry directions. Here, colors are used to distinguish different orbital characteristics (Red: Ce-4*f*; Green: Ce-5*d*; Blue: Al-3*p*), $\Delta_1 \sim \Delta_2$ mark the Dirac band gaps opened by SOC, DC means the Dirac cone. (c) and (d) Quasiparticle band structures for α -Ce₃Al in the same high-symmetry directions as in (a) and (b). Here, Δ_2 and DC mean the renormalized Dirac gap and Dirac cone, respectively.

fermions. These dispersionless flat bands and Dirac cones (or Dirac gaps) are indeed kagome-derived features, instead of a consequence of strong 4*f* electronic correlation or *c* – *f* hybridization effect.

Next, we wonder whether these kagome-related features will be modified by strong electronic correlation. In Fig. 6(c) and (d), the corresponding quasiparticle band structures obtained by DFT + DMFT calculations are shown. First of all, the kagome-derived flat bands are strongly renormalized. The band width is greatly reduced and the central energy level is shifted downward. Second, the Dirac gap Δ_1 is destroyed. Though the Dirac gap Δ_2 still survives, it is slightly shifted toward the Fermi level. Third, the Dirac cone at the H point (DC) is pushed onto the Fermi level and touches the flat bands. The nearby band structure is quite incoherent. As a whole, the influence of 4*f* electronic correlation on the kagome-derived

bands can not be ignored in this case. Our results imply that there should be a competition between the kagome mechanism and the electronic correlation.

V. SUMMARY

In summary, we performed charge fully self-consistent DFT + DMFT calculations to study the detailed electronic structures of α -Ce₃Al and β -Ce₃Al. The band structures, self-energy functions, and valence state histograms of them were determined. Both phases are typical heavy-fermion metals. Their 4*f* electrons tend to be itinerant and strongly hybridize with the conduction electrons. The 4*f* valence state fluctuations are comparable to those in α -Ce. We estimated the single-impurity Kondo temperature T_K and the coher-

ent Kondo temperature T_K^* . We find that $T_K \gg T_K^*$, which agrees with the prediction of Nozières' exhaustion theory and suggests that both phases would retain the protracted Kondo screening state over a wide range of temperature. In addition, clear signatures of kagome metal, including dispersionless flat bands and linearly dispersive bands, are identified in the band structure of α -Ce₃Al. Thus, it is concluded that the α phase of Ce₃Al is a candidate of heavy-fermion kagome metal. This material should provide a fertilizer playground to study the entanglement of topology, Kondo screening, and heavy-fermion

behavior. Further experiments and theoretical studies to validate our predictions are highly desired.

ACKNOWLEDGMENTS

This work was supported by the Natural Science Foundation of China (No. 11874329, 11934020, and 11704347), and the Science Challenge Project of China (No. TZ2016004).

-
- * lihuang.dmft@gmail.com
- ¹ F. Steglich, J. Aarts, C. D. Bredl, W. Lieke, D. Meschede, W. Franz, and H. Schäfer, *Phys. Rev. Lett.* **43**, 1892 (1979).
 - ² O. Stockert, J. Arndt, E. Faulhaber, C. Geibel, H. S. Jeevan, S. Kirchner, M. Loewenhaupt, K. Schmalzl, W. Schmidt, Q. Si, and F. Steglich, *Nat. Phys.* **7**, 119 (2011).
 - ³ G. Pang, M. Smidman, J. Zhang, L. Jiao, Z. Weng, E. M. Nica, Y. Chen, W. Jiang, Y. Zhang, W. Xie, H. S. Jeevan, H. Lee, P. Gegenwart, F. Steglich, Q. Si, and H. Yuan, *Proc. Nat. Acad. Sci.* **115**, 5343 (2018).
 - ⁴ T. Yamashita, T. Takenaka, Y. Tokiwa, J. A. Wilcox, Y. Mizukami, D. Terazawa, Y. Kasahara, S. Kittaka, T. Sakakibara, M. Konczykowski, S. Seiro, H. S. Jeevan, C. Geibel, C. Putzke, T. Onishi, H. Ikeda, A. Carrington, T. Shibauchi, and Y. Matsuda, *Sci. Adv.* **3**, e1601667 (2017).
 - ⁵ H. Q. Yuan, F. M. Grosche, M. Deppe, C. Geibel, G. Sparn, and F. Steglich, *Science* **302**, 2104 (2003).
 - ⁶ G. R. Stewart, *Rev. Mod. Phys.* **56**, 755 (1984).
 - ⁷ H.-H. Lai, S. E. Grefe, S. Paschen, and Q. Si, *Proc. Nat. Acad. Sci.* **115**, 93 (2018).
 - ⁸ M. Dzero, J. Xia, V. Galitski, and P. Coleman, *Annu. Rev. Condens. Matter Phys.* **7**, 249 (2016).
 - ⁹ G. R. Stewart, *Rev. Mod. Phys.* **73**, 797 (2001).
 - ¹⁰ M. Dzero, K. Sun, V. Galitski, and P. Coleman, *Phys. Rev. Lett.* **104**, 106408 (2010).
 - ¹¹ E. Schuberth, M. Tippmann, L. Steinke, S. Lausberg, A. Steppke, M. Brando, C. Krellner, C. Geibel, R. Yu, Q. Si, and F. Steglich, *Science* **351**, 485 (2016).
 - ¹² P. Gegenwart, Q. Si, and F. Steglich, *Nat. Phys.* **4**, 186 (2008).
 - ¹³ Z. F. Weng, M. Smidman, L. Jiao, X. Lu, and H. Q. Yuan, *Rep. Prog. Phys.* **79**, 094503 (2016).
 - ¹⁴ S. Kitagawa, G. Nakamine, K. Ishida, H. S. Jeevan, C. Geibel, and F. Steglich, *Phys. Rev. Lett.* **121**, 157004 (2018).
 - ¹⁵ Y. Li, M. Liu, Z. Fu, X. Chen, F. Yang, and Y.-f. Yang, *Phys. Rev. Lett.* **120**, 217001 (2018).
 - ¹⁶ S. Kittaka, Y. Aoki, Y. Shimura, T. Sakakibara, S. Seiro, C. Geibel, F. Steglich, H. Ikeda, and K. Machida, *Phys. Rev. Lett.* **112**, 067002 (2014).
 - ¹⁷ D. Y. Kim, S.-Z. Lin, F. Weickert, M. Kenzelmann, E. D. Bauer, F. Ronning, J. D. Thompson, and R. Movshovich, *Phys. Rev. X* **6**, 041059 (2016).
 - ¹⁸ C. F. Miclea, M. Nicklas, D. Parker, K. Maki, J. L. Sarrao, J. D. Thompson, G. Sparn, and F. Steglich, *Phys. Rev. Lett.* **96**, 117001 (2006).
 - ¹⁹ J. Paglione, M. A. Tanatar, D. G. Hawthorn, F. Ronning, R. W. Hill, M. Sutherland, L. Taillefer, and C. Petrovic, *Phys. Rev. Lett.* **97**, 106606 (2006).
 - ²⁰ M. Yokoyama, K. Suzuki, K. Tenya, S. Nakamura, Y. Kono, S. Kittaka, and T. Sakakibara, *Phys. Rev. B* **99**, 054506 (2019).
 - ²¹ J. Paglione, M. A. Tanatar, J.-P. Reid, H. Shakeripour, C. Petrovic, and L. Taillefer, *Phys. Rev. Lett.* **117**, 016601 (2016).
 - ²² Y. P. Liu, Y. J. Zhang, J. J. Dong, H. Lee, Z. X. Wei, W. L. Zhang, C. Y. Chen, H. Q. Yuan, Y.-f. Yang, and J. Qi, *Phys. Rev. Lett.* **124**, 057404 (2020).
 - ²³ N. P. Armitage, E. J. Mele, and A. Vishwanath, *Rev. Mod. Phys.* **90**, 015001 (2018).
 - ²⁴ S. Dzsaber, L. Prochaska, A. Sidorenko, G. Eguchi, R. Svagera, M. Waas, A. Prokofiev, Q. Si, and S. Paschen, *Phys. Rev. Lett.* **118**, 246601 (2017).
 - ²⁵ S. E. Grefe, H.-H. Lai, S. Paschen, and Q. Si, *Phys. Rev. B* **101**, 075138 (2020).
 - ²⁶ J. Schweizer, F. Givord, J.-X. Boucherle, F. Bourdarot, and E. Ressouche, *J. Phys.: Condensed Matter* **20**, 135204 (2008).
 - ²⁷ K. Andres, J. E. Graebner, and H. R. Ott, *Phys. Rev. Lett.* **35**, 1779 (1975).
 - ²⁸ H. Nakamura, Y. Kitaoka, K. Asayama, and J. Flouquet, *J. Phys. Soc. Japan* **57**, 2644 (1988).
 - ²⁹ M. Sera, T. Satoh, and T. Kasuya, *J. Magn. Magn. Mater.* **63-64**, 82 (1987).
 - ³⁰ Y.-Y. Chen, J. M. Lawrence, J. D. Thompson, and J. O. Willis, *Phys. Rev. B* **40**, 10766 (1989).
 - ³¹ Y. Y. Chen, Y. D. Yao, B. C. Hu, C. H. Jang, J. M. Lawrence, H. Huang, and W. H. Li, *Phys. Rev. B* **55**, 5937 (1997).
 - ³² W.-H. Li, J. C. Peng, Y.-C. Lin, K. C. Lee, J. W. Lynn, and Y. Y. Chen, *J. Appl. Phys.* **83**, 6426 (1998).
 - ³³ D. Singh, S. Yadav, D. Venkateshwarlu, M. Gangrade, S. S. Samatham, and V. Ganesan, *Mater. Res. Express* **1**, 046114 (2014).
 - ³⁴ P. Nozières, *Eur. Phys. J. B* **6**, 447 (1998).
 - ³⁵ S. Sachdev, *Phys. Rev. B* **45**, 12377 (1992).
 - ³⁶ G. Kotliar, S. Y. Savrasov, K. Haule, V. S. Oudovenko, O. Parcollet, and C. A. Marianetti, *Rev. Mod. Phys.* **78**, 865 (2006).
 - ³⁷ A. Georges, G. Kotliar, W. Krauth, and M. J. Rozenberg, *Rev. Mod. Phys.* **68**, 13 (1996).
 - ³⁸ E. A. Goremychkin, H. Park, R. Osborn, S. Rosenkranz, J.-P. Castellán, V. R. Fanelli, A. D. Christianson, M. B. Stone, E. D. Bauer, K. J. McClellan, D. D. Byler, and J. M. Lawrence, *Science* **359**, 186 (2018).
 - ³⁹ J. H. Shim, K. Haule, and G. Kotliar, *Science* **318**, 1615 (2007).
 - ⁴⁰ L. Huang and H. Lu, *Phys. Rev. B* **99**, 045122 (2019).
 - ⁴¹ H. Lu and L. Huang, *Phys. Rev. B* **98**, 195102 (2018).
 - ⁴² K. Haule, C.-H. Yee, and K. Kim, *Phys. Rev. B* **81**, 195107 (2010).
 - ⁴³ H. Lu and L. Huang, *Phys. Rev. B* **94**, 075132 (2016).
 - ⁴⁴ P. Blaha, K. Schwarz, G. Madsen, D. Kvasnicka, and J. Luitz, *WIEN2k, An Augmented Plane Wave + Local Orbitals Program for Calculating Crystal Properties* (Karlheinz Schwarz, Techn. Universität Wien, Austria, 2001).

- ⁴⁵ J. P. Perdew, K. Burke, and M. Ernzerhof, *Phys. Rev. Lett.* **77**, 3865 (1996).
- ⁴⁶ K. Haule, *Phys. Rev. Lett.* **115**, 196403 (2015).
- ⁴⁷ K. Haule, *Phys. Rev. B* **75**, 155113 (2007).
- ⁴⁸ P. Werner, A. Comanac, L. de' Medici, M. Troyer, and A. J. Millis, *Phys. Rev. Lett.* **97**, 076405 (2006).
- ⁴⁹ E. Gull, A. J. Millis, A. I. Lichtenstein, A. N. Rubtsov, M. Troyer, and P. Werner, *Rev. Mod. Phys.* **83**, 349 (2011).
- ⁵⁰ H. Lu and L. Huang, *Phys. Rev. B* **95**, 155140 (2017).
- ⁵¹ K. Haule, S. Kirchner, J. Kroha, and P. Wölfle, *Phys. Rev. B* **64**, 155111 (2001).
- ⁵² P. Zhang, B. Liu, S. Zhang, K. Haule, and J. Dai, "Protracted Kondo coherence with dilute carrier density in Cerium based nickel pnictides," (2019), [arXiv:1909.13251 \[cond-mat\]](#).
- ⁵³ Y. Luo, F. Ronning, N. Wakeham, X. Lu, T. Park, Z.-A. Xu, and J. D. Thompson, *Proc. Nat. Acad. Sci.* **112**, 13520 (2015).
- ⁵⁴ M. Jarrell and J. Gubernatis, *Phys. Rep.* **269**, 133 (1996).
- ⁵⁵ Z. Lin, J.-H. Choi, Q. Zhang, W. Qin, S. Yi, P. Wang, L. Li, Y. Wang, H. Zhang, Z. Sun, L. Wei, S. Zhang, T. Guo, Q. Lu, J.-H. Cho, C. Zeng, and Z. Zhang, *Phys. Rev. Lett.* **121**, 096401 (2018).
- ⁵⁶ L. Ye, M. K. Chan, R. D. McDonald, D. Graf, M. Kang, J. Liu, T. Suzuki, R. Comin, L. Fu, and J. G. Checkelsky, *Nat. Commun.* **10**, 4870 (2019).
- ⁵⁷ J.-X. Yin, S. S. Zhang, H. Li, K. Jiang, G. Chang, B. Zhang, B. Lian, C. Xiang, I. Belopolski, H. Zheng, T. A. Cochran, S.-Y. Xu, G. Bian, K. Liu, T.-R. Chang, H. Lin, Z.-Y. Lu, Z. Wang, S. Jia, W. Wang, and M. Z. Hasan, *Nature* **562**, 91 (2018).
- ⁵⁸ L. Ye, M. Kang, J. Liu, F. von Cube, C. R. Wicker, T. Suzuki, C. Jozwiak, A. Bostwick, E. Rotenberg, D. C. Bell, L. Fu, R. Comin, and J. G. Checkelsky, *Nature* **555**, 638 (2018).
- ⁵⁹ Q. Wang, Q. Yin, and H. Lei, *Chin. Phys. B* **29**, 017101 (2020).
- ⁶⁰ K. Kim, J. Seo, E. Lee, K. T. Ko, B. S. Kim, B. G. Jang, J. M. Ok, J. Lee, Y. J. Jo, W. Kang, J. H. Shim, C. Kim, H. W. Yeom, B. Il Min, B.-J. Yang, and J. S. Kim, *Nat. Mater.* **17**, 794 (2018).
- ⁶¹ E. Liu, Y. Sun, N. Kumar, L. Muechler, A. Sun, L. Jiao, S.-Y. Yang, D. Liu, A. Liang, Q. Xu, J. Kroder, V. Süß, H. Borrmann, C. Shekhar, Z. Wang, C. Xi, W. Wang, W. Schnelle, S. Wirth, Y. Chen, S. T. B. Goennenwein, and C. Felser, *Nat. Phys.* **14**, 1125 (2018).
- ⁶² Q. Wang, Y. Xu, R. Lou, Z. Liu, M. Li, Y. Huang, D. Shen, H. Weng, S. Wang, and H. Lei, *Nat. Commun.* **9**, 3681 (2018).
- ⁶³ J.-X. Yin, S. S. Zhang, G. Chang, Q. Wang, S. S. Tsirkin, Z. Guguchia, B. Lian, H. Zhou, K. Jiang, I. Belopolski, N. Shumiya, D. Multer, M. Litskevich, T. A. Cochran, H. Lin, Z. Wang, T. Neupert, S. Jia, H. Lei, and M. Z. Hasan, *Nat. Phys.* **15**, 443 (2019).
- ⁶⁴ R. Yang, T. Zhang, L. Zhou, Y. Dai, Z. Liao, H. Weng, and X. Qiu, *Phys. Rev. Lett.* **124**, 077403 (2020).
- ⁶⁵ Z. Lin, C. Wang, P. Wang, S. Yi, L. Li, Q. Zhang, Y. Wang, Z. Wang, Y. Sun, Z. Sun, J.-H. Cho, C. Zeng, and Z. Zhang, "Dirac Fermions in Antiferromagnetic FeSn Kagome Lattices with Combined Space Inversion and Time Reversal Symmetry," (2019), [arXiv:1906.05755 \[cond-mat\]](#).
- ⁶⁶ M. Kang, L. Ye, S. Fang, J.-S. You, A. Levitan, M. Han, J. I. Facio, C. Jozwiak, A. Bostwick, E. Rotenberg, M. K. Chan, R. D. McDonald, D. Graf, K. Kaznatcheev, E. Vescovo, D. C. Bell, E. Kaxiras, J. van den Brink, M. Richter, M. Prasad Ghimire, J. G. Checkelsky, and R. Comin, *Nat. Mater.* **19**, 163 (2020).
- ⁶⁷ Z. Liu, M. Li, Q. Wang, G. Wang, C. H. P. Wen, K. Jiang, X. Lu, S. Yan, Y. Huang, D. Shen, J. Yin, Z. Wang, Z. Yin, H. Lei, , and S. Wang, "Orbital-Selective Dirac Fermions and Extremely Flat Bands in the Nonmagnetic Kagome Metal CoSn," (2020), [arXiv:2001.11738 \[cond-mat\]](#).
- ⁶⁸ M. Kang, S. Fang, L. Ye, H. C. Po, J. Denlinger, C. Jozwiak, A. Bostwick, E. Rotenberg, E. Kaxiras, J. G. Checkelsky, and R. Comin, "Topological flat bands in frustrated kagome lattice CoSn," (2020), [arXiv:2002.01452 \[cond-mat\]](#).
- ⁶⁹ Y. Zhang, H. Lu, X. Zhu, S. Tan, W. Feng, Q. Liu, W. Zhang, Q. Chen, Y. Liu, X. Luo, D. Xie, L. Luo, Z. Zhang, and X. Lai, *Sci. Adv.* **4**, eaao6791 (2018).